Accepted Manuscript

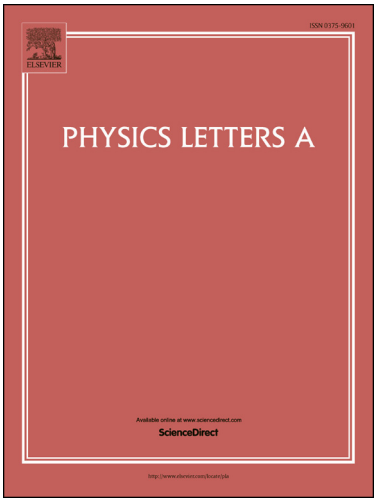

Boundary condition-selective length dependence of the flexural rigidity of microtubules

Jin Zhang, Chengyuan Wang

PII: S0375-9601(17)30423-1
DOI: http://dx.doi.org/10.1016/j.physleta.2017.04.040
Reference: PLA 24484

To appear in: *Physics Letters A*

Received date: 10 February 2017
Revised date: 25 April 2017
Accepted date: 28 April 2017

Please cite this article in press as: J. Zhang, C. Wang, Boundary condition-selective length dependence of the flexural rigidity of microtubules, *Phys. Lett. A* (2017), http://dx.doi.org/10.1016/j.physleta.2017.04.040

Highlights

- Real boundary condition imposed on microtubules (MTs) in experiments is described.
- Length dependence of the flexural rigidity of MTs is boundary condition-selective.
- Boundary condition-selective phenomenon is mainly due to imperfect boundary effect.

Boundary condition-selective length dependence of the flexural rigidity of microtubules

Jin Zhang[1*], Chengyuan Wang[2*]

[1] Shenzhen Graduate School, Harbin Institute of Technology, Shenzhen 518055, China

[2] Zienkiewicz Centre for Computational Engineering, College of Engineering, Swansea University, Bay Campus, Fabian Way, Swansea, Wales SA2 8EN, UK

Abstract: Length-dependent flexural rigidity (FR) is observed experimentally for microtubules (MTs) subjected to certain boundary conditions. To shed some light on this unique feature, we have studied the FR of MTs with different boundary conditions. A molecular structural mechanics method is employed to accurately describe the real boundary conditions imposed on MTs in experiments. Some of component protofilaments of MTs are blocked at the ends while others are free. In addition, linked kinesin is treated as an elastic body rather than a rigid body. Our simulations show that for relatively long MTs having a length comparable to those measured in experiments the length-dependent rigidity is detected only for those with fixed-free and fixed-fixed ends, which is consistent with the experimental observation. To capture the physics leading to the above phenomenon, Timoshenko beam model is adopted accounting for both transverse shear effect (TSE) and imperfect boundary effect (IBE). Comparison between TSE and IBE indicates that the boundary condition-selective length-dependence achieved for the FR of relatively long MTs is primarily a result of the influence of IBE rather than TSE.

Keywords: Microtubule; Flexural rigidity; Length dependence; Boundary condition

*Corresponding authors.

E-mail address: jinzhang@hit.edu.cn (J. Zhang); chengyuan.wang@swansea.ac.uk (C. Wang).

1. Introduction

Microtubules (MTs) are protein filaments that exist universally in eukaryotic cells. MTs are composed of α- and β-tubulin heterodimers [1]. These dimers attach with each other longitudinally in a head-to-tail fashion constructing a beam-like protofilament. A number of parallel protofilaments are aligned to form an elegant chiral MT structure via the lateral interaction between adjacent protofilaments. In MTs the adjacent protofilaments are shifted relatively to each other longitudinally, resulting in a helical order in the lateral direction. This unique feature is characterised by the helix-start number *S*. Thus, different MT types can be represented by the notation of *N_S* with *N* being the number of protofilaments included in the MT wall. According to the experimental study [2], 13_3 MTs are the most frequently observed type *in vivo*. Due to the unique molecular structures, MTs play an important role in the mechanics of the cell due to their high axial mechanical stiffness and transverse flexibility. For example, MTs are responsible for maintaining the cell structural stiffness, functioning as a track for motor proteins to transport organelles and facilitating cell division [3-5]. The mechanical properties of MTs thus become a current topic of great interest in the areas of cell mechanics and nano-biomaterials [1]. Specifically, among these properties the flexural rigidity (FR) is an important parameter for characterising bending [6-8], buckling [9-17], vibration [18-24] and wave propagation [25-28] of MTs.

In the past two decades, various experimental techniques have been employed to measure the FR of MTs, such as optical tweezers [29, 30], atomic force microscope [6, 31], hydrodynamic flow [32, 33] and thermal fluctuations [32, 34-37]. To examine the FR of an MT *in vitro*, one can fluctuate a free-standing MT through the thermal fluctuation method [36, 37] or probe the MT with a direct (passive or active) force, where different constraints are enforced on the ends of the tested MTs [6, 31, 35, 38]. Usually, the ends of MTs tested *in vitro* are covalently

grafted on a microstructured substrate [6, 31, 35, 38] (see Fig. 1a) or connected to the kinesin molecule, whose structure contains a globular head, a stalk-like central region and a globular end tail [10, 39] (see Fig. 1c). Mechanics models are thus required for MTs with different end conditions to interpret the experimental data (e.g., buckling force or persistence length) and quantify the effective FR. A free-standing MT can be typically modelled as an elastic beam with free boundary conditions; an MT attached to the substrate (Fig. 1a) can normally be treated as a beam with perfectly clamped boundaries (see Fig. 1b) [6, 31, 35, 38]; the one linked to the kinesin (Fig. 1c) is usually described as a perfect simply supported beam (see Fig. 1d) [10, 39]. In Tab. 1 we have summarized the FR of MTs measured by different experimental methods. From Tab. 1 some experiments reported the length-dependent FR, while others claimed the constant FR independent with the contour length. Moreover, the achieved length dependence of the FR seems to be sensitive to the boundary conditions of MTs. For instance, the length-dependent FR is found for fixed-free and fixed-fixed ends, while the constant FR is achieved for pinned-pinned and free-free boundary conditions. This observation infers a possible correlation between the boundary conditions and the length-dependent FR. Motivated by this idea, we are interested in further examining the issue in detail and capturing the physical origin of the experimentally observed length dependence of the FR. In the literature, there are three theories proposed to explain the length dependence of the FR of MTs: (1) the effect of transverse shear deformation proposed for short beams in Timoshenko beam theory [6, 20, 31, 35], (2) the effect of the imperfect constrains at MTs' ends (imperfect boundary conditions) [18, 40], and (3) the nonlocal effect [8, 13-15, 25, 27]. According to our recent analyses [41, 42] the nonlocal effect actually has no effect on the mechanics of relatively long MTs. Thus the former two effects

would be responsible for the length-dependent FR. It thus becomes essential in the present study to identify the key factor that controls the length dependence of the FR.

In this paper, the FR of MTs whose ends are free or attached to the substrate or linked to kinesin molecules has been studied based on the molecular structural mechanics (MSM)-based vibration analysis. The concept of the MSM method originates from the observation of geometric similarities between the coarse-grained molecular dynamics (MD) model of MTs and macroscopic space frame structures [18, 41, 42]. As the MSM model ignores the thermal vibration of the atoms, it can economise the computational cost. In the meantime, this technique still retains the ability to account for the effect of the molecular structures on the mechanical responses of biomaterials. In the present MSM study the length dependence of the FR of MTs is found to be significantly boundary condition-selective, which is similar to the experimental observation. This phenomenon however cannot be explained by the conventional Timoshenko beam model considering the transverse shear effect (TSE) only. The general boundary conditions is then adopted for Timoshenko beam model, which enables one to quantify both TSE and the imperfect boundary effect (IBE) on the FR.

2. **MSM model for the vibrations of MTs**

MSM method [18, 41, 42] will be employed in the present study for the vibration analysis of MTs. The robustness and efficiency of this technique have been demonstrated in modelling the static deformation (tension, torsion and bending) [41], the elastic buckling [42] and the free vibration of MTs [18]. The calculated results of Young's modulus, shear modulus, bending stiffness and critical buckling force of MTs are in good agreement with available simulation and

experiment results [41, 42]. In this work, the MSM method will be extended to the vibration of MTs whose ends attached to the substrate or linked to kinesin molecules.

2.1. A brief review of MSM method for MTs

In the MSM method, the interactions between two neighbouring constitutive monomers (i.e., αβ bond along the protofilament direction and αα or ββ bond along the helical direction) are simulated as equivalent structural beams with circular cross-sections [41]. According to the theory of structural mechanics, only three stiffness parameters, i.e., the extensional stiffness $E_b A_b$, the bending stiffness $E_b I_b$, and the torsional stiffness $G_b J_b$, need to be determined for the analysis of the deformation of the MSM model. Here, E_b and G_b are, respectively, Young's modulus and shear modulus of the beam; A_b, I_b and J_b are, respectively, the area, the moment of inertia and the polar inertia of the beam cross-section. Based on the energy equivalence between local potential energies in computational chemistry and elemental strain energies in structural mechanics, the extensional stiffness, the bending stiffness and the torsional stiffness for an equivalent beam can be determined from force field constants in molecular mechanics via the following equations $E_b A_b = k_r l$, $E_b I_b = k_\phi l$ and $G_b J_b = k_\tau l$. Here, k_r, k_ϕ and k_τ are the force constants for bond stretching, bond angle bending and bond torsion, respectively; l is the length of the equivalent beam. The values of these constants are different for αβ along the protofilament direction and αα or ββ bond along the helical direction and can be taken from Ref. [43]. These parameter values have been proven to be accurate through a series of MD simulations and MSM simulations on the mechanical behaviours of MTs [18, 41-43]. In addition, the mass of each (α or β) tubulin monomer m_t is taken as 55kDa [44] and acts at the mass centre of the monomer.

After applying the above equivalent beam model to all the tubulin-tubulin bonds we will finally turn an MT into a space-frame structure, where the overall mass matrices **M** and stiffness matrices **K** of the MSM model are generated based on the mass and stiffness of the individual equivalent beams. The equation of motion of the MT can then be written as $\mathbf{M}\ddot{\mathbf{x}}+\mathbf{K}\mathbf{x}=\mathbf{0}$, where $\ddot{\mathbf{x}}$ is the second time derivative of the displacement $\mathbf{x}$, i.e., the acceleration. This equation of motion further gives the eigenequation as $(\mathbf{K}-\omega^2\mathbf{M})\mathbf{x}=\mathbf{0}$, where ω is the angular natural frequency. The frequency of an MT can be obtained by solving this eigenvalue problem. The calculation was implemented via the block Lanczos algorithm [18, 45].

It is noted that in the experiments where MTs were attached to the substrate [6, 31, 35, 38] (see Fig. 1a) only some of the prtofilaments' ends are blocked by the substrate, while the others are free to move. In addition, when MTs were linked to the kinesin molecule their ends may not be simplified as perfect simply supported boundaries [10, 39], since the kinesin is actually an elastic rather than rigid body [46]. In modelling MTs attached to the substrate (see Fig. 1a), the effect of the boundary condition will be studied by changing the number of filaments blocked by the substrate. Meanwhile, for MTs linked to kinesin molecules (see Fig. 1c), the effect of the boundary condition will be mimicked by connecting the filament (represented by a beam element in the MSM model) to a bar element, representing the elastic kinesin molecules. The elastic property of the kinesin molecules (bar elements) thus must be evaluated before we can start performing the simulations.

2.2. Elastic property of kinesin

In this subsection, we will measure the elastic property of a kinesin molecule. Kinesin molecules are normally formed bearing two large globular heads that allow attachment to MTs, a flexible stalk-like central region interrupted by stiffer double-helical coiled-coils and two small

globular end tails (see Fig. 2a). Conceptually, the stalk-like central region is the structure domain of the whole kinesin and thus mainly characterises the elastic behaviours of the whole kinesin [46, 47]. Thus, in this study we will mainly focus on the elastic property of the stalk-like central region. To reach this goal we will perform a tensile test for a segment of the stalk using the molecular mechanics (MM) simulations.

In this study, the geometry of the segment of the stalk with a length L_t of ~47 Å is taken from the standard protein data bank (PDB) file, 3KIN.pdb, available from the RCSB Protein Data Bank [48]. In the MM simulations, one end of the stalk segment was fixed while the other end was pulled along the axial direction (see Fig. 2c). MM simulations were thus performed with the Gaussian program using the powerful universal force field (UFF) [49]. The potential components described in the UFF with specific parameters are defined as

$$E_{total} = E_R + E_\theta + E_\phi + E_\omega + E_{vdW} + E_{el} . \quad (1)$$

The valence interactions consist of two items, i.e., (1) bond stretching (E_R), which is a harmonic term and (2) angular distortions including bond angle bending (E_θ), described by a three-term Fourier cosine expansion, dihedral angle torsion (E_ϕ), and inversion terms (out-of-plane bending) (E_ω). Here, E_ϕ and E_ω are described by cosine-Fourier expansion terms. The nonbonded interactions involve van der Waals (E_{vdW}) and electrostatic (E_{el}) terms. E_{vdW} is described by a Lennard-Jones potential and E_{el} is described by a Coulombic term. The functional form of these energy terms is given as follows:

$E_R = k_1(r - r_0)^2$, $E_\theta = k_2(C_0 + C_1\cos\theta + C_2\cos 2\theta)^2$, $C_0 = -4C_2\cos\theta_0$, $C_1 = C_2(2\cos^2\theta_0 + 1)$,

$C_2 = \frac{1}{4\sin^2\theta}$, $E_\phi = k_3(1 \pm \cos n\phi)$, $E_\omega = k_4[1 \pm \cos(n\chi - \chi_0)]$, $E_{vdW} = \delta\left[\left(\frac{r_1}{r}\right)^{12} - 2\left(\frac{r_1}{r}\right)^6\right]$,

$$E_{el} = \frac{q_i q_j}{\varepsilon_0 r_{ij}}. \quad (2)$$

Here, k_1, k_2, k_3 and k_4 are force constants, θ_0 is the the natural bond angle, δ is the van der Waals well depth, r_1 is the van der Waals length, q_i is the net charge of an atom, ε_0 is the dielectric constant, and r_{ij} is the distance between two atoms. The E_{el} term is a Coulombic term and is nonzero in the present study. The Gaussian program assigned the atomic charges automatically based on the atom types. The atomic charges are assigned according to "Qeq algorithm" presented by Ref. [50]. The values of these parameters in Eq. 2 can be found in Ref. [49]. This UFF has been used for various nanoscale materials including deoxyribonucleic acid [51], α(β) tubulin monomer [52], carbon nanotube [53] and graphene sheet [54].

In Fig. 2d we plot the relationship between the axial strain ε and the stored strain energy U of the stalk segment during the tensile test, where the small strain $\varepsilon < 1\%$ was considered. We can see from Fig. 2d that at the small deformation U increases almost quadratically with ε. This U-ε relationship in the small deformation range offers a means to calculate the effective elastic properties of stalk segment. In order to obtain this effective elastic properties, a continuum bar model with an effective cross-sectional area A and Young's modulus E was used (see Fig. 2b). The tensile rigidity $Y = E \cdot A$ of the segment of the stalk can thus be evaluated as $Y = (\partial^2 U / \partial \varepsilon^2) / L_t$. The fitted Y of the stalk is about 4 nN.

3. **Continuum beam models for the vibrations of MTs**

Although atomistic and molecular scale methods, e.g., MSM [18, 41, 42], anisotropic elastic network model [55] and MD simulations [56, 57], have been used to understand the mechanical behaviours of MTs, due to the size and time limitation of atomistic and molecular

scale methods themselves, they are only applicable for relatively short MTs or MT segments. Thus, the continuum models, especially the beam models, are often used to study the mechanical behaviours of the whole MTs [8, 11-13, 20, 21]. In the framework of the continuum mechanics, an MT can be descried as an Euler-Bernoulli beam at its simplest approximation. The dynamics equation for the transverse vibration of an MT can be expressed as [58]

$$D\frac{\partial^4 w}{\partial x^4}+\rho\frac{\partial^2 w}{\partial t^2}=0\,. \tag{3}$$

Here $w\equiv w(x,t)$ is the transverse deflection, x is the axial coordinate, t is the time, ρ is the mass density per uniaxial length [18], and D is the FR. The angular natural frequency of an MT obtained from Eq. 3 can be expressed as [58] $\omega=\sqrt{D\gamma^4/(\rho L^4)}$, where L is the length of MTs and γ is a dimensionless parameter depending on the boundary conditions of MTs. γ equals to 1.875, 3.142, 4.730 and 4.730, respectively, for MTs with perfectly fixed-free, pinned-pinned, fixed-fixed and free-free boundary conditions. Following equation can be obtained from $\omega=\sqrt{D\gamma^4/(\rho L^4)}$, which enables one to predict the FR of MTs

$$D=\omega^2 L^4\rho/\gamma^4\,. \tag{4}$$

Equation 4 will be used in the present study to calculate the effective FR of MT from the angular natural frequency obtained in the above-mentioned MSM and below continuum mechanics model.

On the other hand, recent direct atomistic and molecular scale simulations have shown that the shear modulus of MTs is usually two orders of magnitude lower than their Young's modulus [41, 55]. As a result, the TSE neglected by Euler-Bernoulli beam model is expected to play a crucial role in MT mechanics. To consider the influence of TSE, Timoshenko beam model

was used to describe MTs [6, 12, 13, 20, 42]. Based on Timoshenko beam theory, the dynamics equation for the transverse vibration of an MT reads [58]

$$D\frac{\partial^2\phi}{\partial x^2}-K_sGA\left(\phi+\frac{\partial w}{\partial x}\right)=0,$$

$$K_sGA\left(\frac{\partial\phi}{\partial x}+\frac{\partial^2 w}{\partial x^2}\right)-\rho\frac{\partial^2 w}{\partial t^2}=0. \quad (5)$$

Here, $\phi\equiv\phi(x,t)$ is the rotation angle, G is the shear modulus of MTs, whose value can be obtained from our recent study [41], A is the cross-sectional area of MTs, K_s is a geometrical correction factor and is taken as 0.72 for MTs [35]. The boundary conditions of the MTs with perfect boundaries assumed in the previous experiments [6, 10, 31, 35, 38, 39] are listed in Tab. 2. We assume the solutions of Eq. 3 and Eq. 5 as $w(x,t)=W(x)e^{i\omega t}$ and $\phi(x,t)=\Phi(x)e^{i\omega t}$. After substituting these solutions into Eq. 3 or Eq. 5 together with the corresponding boundary conditions listed in Tab. 2, we can obtain the frequency ω of MTs numerically by solving the resultant ordinary differential equations through the differential quadrature method [59].

4. Results and discussion

Based on MSM method, in this section we will study the vibration behaviours of 13_3 MTs whose length ranges from 100 nm to 10 μm. Specifically, in terms of the length of MTs we have studied two cases: (1) relatively short MTs whose length L is smaller than 1 μm, and (2) relatively long MTs (L > 1 μm), whose length is comparable to those measured in experiments. With the aid of the technique proposed above (Eq. 4) we have thus studied the influence of the length on the FR of MTs. A modified Timoshenko beam model considering the TSE and IBE

simultaneously was also built to explain the simulation results and explore the main factor responsible for the length-dependent FR observed in simulations and experiments.

4.1 Comparison between different beam theories

In addition to the classical Timoshenko beam model illustrated above (Eq. 5), some modified Timoshenko beam models on the basis of higher order continuum mechanics theories, e.g., nonlocal elasticity theory and modified couple stress (MCS) theory, have been proposed recently to study the mechanical behaviours of MTs [12, 13]. In this subsection, we will compare the classical and modified Timoshenko beam models with MM simulations to reveal the reasons for the length dependence of FR observed in MM simulations. To exclude the influence of the boundary conditions from the length-dependent FR, in this study we selected the free-free MT as an example. After obtaining the angular natural frequency ω from the MSM method, we can calculate the FR D of the simulated MTs using Eq. 4. In Fig. 3 we present the obtained FR of MTs with different lengths. To better illustrate the result, in Fig. 3 D is normalized by the FR of a sufficiently long MT (D_0), in which the TSE is excluded. From Fig. 3 we can see that the FR obtained in MSM simulations decreases as the length of MTs decreases. Similar length dependence of the FR is also detected in other molecular-level simulation methods, e.g., anisotropic elastic network (AEN) method [55] (see Fig. 3). Specifically, we also find that our MSM results coincide with the AEN results very well, denoting that the present MSM simulations are reliable in studying the length dependence of FR. To explain the length dependence of FR observed in MM simulations, in Fig. 3 we also show the results calculated from the classical Timoshenko beam model only considering TSE and also the modified Timoshenko beam models, in which the TSE and small-scale effects are simultaneously taken into account. The modified Timoshenko beam models of MTs considered here are developed

based on the nonlocal elasticity theory and the MCS theory (see the Appendix). In the calculation, the cross-sectional area $A = 180\ \text{nm}^2$ [55], the FR of sufficiently long MTs $D_0 = 9\times10^{-24}\ \text{N m}^2$ [41, 55], the shear modulus $G = 45\ \text{MPa}$ [41, 55, 56] and the mass density $\rho = 2.9\times10^{-10}\ \text{g m}^{-1}$ [18]. Moreover, in the modified Timoshenko beam models we take $e_0 a = 10\ \text{nm}$ and $l = 10\ \text{nm}$ as an example. From Fig. 3 we can see that the classical Timoshenko beam model fits MM simulations very well, while substantial deviation from MM simulations is observed for both two modified Timoshenko beam models. This result indicates that the length-dependent FR detected in MM simulations (both MSM and AEN simulations) is mainly attributed to the TSE and the classical Timoshenko beam model is adequate in studying the FR of MTs. Similar conclusions were also drawn in our studies on the bending and buckling of MTs [41, 42].

4.2 Equivalent FR of relatively short MTs

In the above study, we have considered an MT without restriction at ends. In reality, the ends of MTs tested *in vitro* are covalently grafted on a microstructured substrate (see Fig. 1a) or connected to the kinesin molecules. To more accurately reflect the real *in vitro* experiment conditions of MTs, we have blocked only three (out of thirteen) filaments at the ends and considered the elasticity of the linked kinesin. In Fig. 4 we plot the length dependence of the FR for MTs with different boundary conditions. Here, to better illustrate the result, D is normalized by D_0, i.e., D/D_0, where D_0 is the FR of a sufficiently long MT with all its filaments being blocked at ends or linked to a rigid kinesin. In other words, the TSE and IBE are both excluded in D_0. We can see from Fig. 4 that when the length of MTs is relatively small ($L < 1\ \mu$m) the length-dependent phenomenon of the FR is observed to be significant for all MTs, irrespective of their boundary conditions. For example, when L increases from ~100 nm to ~1 μm, D/D_0 is

found to increase from 0.33 to 0.85 for fixed-free MTs, from 0.21 to 0.77 for fixed-fixed MTs, from 0.23 to 1 for pinned-pinned MTs and from 0.6 to 1 for free-free MTs. Obviously, the length dependence of the FR is most significant for MTs with pinned-pinned boundary conditions. Their D/D_0 is raised by a factor of more than three in Fig. 4. As we mentioned before the theory of the transverse shear deformation has been widely used to explain the length dependence of the FR of MTs. In this work, D/D_0 is calculated again based on the Timoshenko beam theory (Eq. 5) by using the same material properties that we utilized above. The obtained results are represented by the dashed lines in Fig. 4 and show the trend similar to ones given by MSM. However, the theoretical results (dashed lines) are substantially greater than the MSM simulations (solid circles) for different boundary conditions. The discrepancy between these two techniques infers that there should exist other physical mechanisms in determining the length-dependent FR observed in simulations and experiments [6, 31, 35, 38].

4.3 Modified Timoshenko beam model considering IBE of MTs

In our previous study for the cantilevered MTs [18], the influence of the imperfect boundary conditions is also found to play an important role in controlling the length dependence of FR. To examine its impact on MTs with different ends, it is of importance to study real deformed shape of MTs, which gives more reliable description of the boundary conditions imposed in experiments. In Figs. 5a and 5c we respectively show the mode shape of fixed-fixed and pinned-pinned MTs studied in the present MSM simulations. Fig. 5a indicates that for the fixed-fixed MTs attached to the substrate, some tubulin monomers also have torsional displacements relative to the blocked filaments, which clearly shows that the perfectly clamped boundary condition cannot describe the actual boundary condition of the experimentally "fixed" end of MTs. To take these relative torsional displacements into account, we assume that the

"fixed" end of MTs is constrained by a torsional spring with the coefficient of k_θ rather than perfectly fixed (see Fig. 5b). In addition, for the pinned-pinned MTs when the elasticity of the kinesin is considered relative transverse displacements are achieved for the tubulin monomers linked to the kinesin. This observation is in contrast to the zero transverse displacement assumed in the previous studies [10, 39]. Thus the perfect simply supported boundary condition should be abandoned for experimentally "pinned" end of MTs. Considering the relative transverse displacements of the "pinned" end, we assume that the "pinned" end of MTs is constrained by a linear spring with the coefficient of k_x (see Fig. 5d). Under these circumstances, a general boundary condition should be introduced for MTs modelled as Timoshenko beams. In continuum mechanics modelling considering the effect of the torsional spring or the linear spring automatically modifies the boundary conditions for the fixed-fixed, fixed-free and pinned-pinned MTs. These modified (imperfect) boundary conditions are tabulated in Tab. 2. It should be pointed out that the equivalent stiffness of the torsional and linear springs utilized here is obtained by fitting the continuum mechanics solution (Eq. 5 and the modified boundary conditions in Tab. 2) to the MSM results. Similar treatment was also employed in our previous study [18] of the dynamics behaviours of the cantilevered MTs with imperfect boundary conditions.

With the aid of the Timoshenko beam model (Eq. 5) together with the modified boundary conditions in Tab. 2 we can examine the influence of the TSE and the IBE simultaneously on the FR. When these two factors are both considered, in Fig. 4 (solid lines) we plot the theoretical results of the normalized FR D/D_0 against the length L of MTs. We can see from Fig. 4 that the continuum mechanics results agree with the MSM results very well. These results and those shown in Fig. 4 manifested that the IBE can be another important physical origin that leads to the

length dependence of the FR found in experiments for MTs. Thus, for the first time in the literature the present work shows that the IBE as well as the TSE should be primarily responsible for the length-dependent FR of MTs with different end constrains (fixed-free, fixed-fixed and pinned-pinned ends).

4.4 Equivalent FR of relatively long MTs

It is worth mentioning that the above MSM studies were limited to MTs with a length smaller than 1 μm due to the computational cost limitation. However, long MTs with a length greater than 1 μm are usually considered in experiments [35]. It is thus required to find a cost-effective model to deal with the long MTs at relatively low cost. As shown above, the modified Timoshenko beam model is able to reproduce the results given by the MSM model, which suggests that the Timoshenko beam model can be efficiently used to correctly account for TSE and IBE of short MTs. It is these unique features that distinguish MTs from classical Euler beams with perfect boundary conditions. Thus, in what follows, this modified beam model will be further extended to the study of the long MTs ($L > 1$ μm) where the influence of TSE and IBE would remain unchanged or become less pronounced. For these long MTs the normalized FR D/D_0 obtained based on the modified beam model is plotted in Fig. 4 (solid lines) as a function of their length L. We can see from Fig. 4 that the length-dependence of the FR for relatively long MTs is controlled primarily by their boundary conditions. For example, when L increases from 1 μm to 10 μm D/D_0 has nearly a constant value close to one for pinned-pinned and free-free MTs. It however varies from 0.77 to 1 for fixed-free MTs and from 0.77 to 1 for fixed-fixed MTs In other words, for long MTs studied in experiments the FR is independent of the length as far as pinned-pinned or free-free ends are concerned. However, the length dependence of FR becomes significant when fixed-free MTs and fixed-fixed MTs are considered. These numerical results

are found to be in accordance with the experimental data showing that the modified beam model is able to provide a theoretical explanation for the experimental observation in Refs. [6, 31, 35, 38] (see Tab. 1).

4.5 Comparison between TSE and IBE

It was shown before that both TSE and IBE have a significant role in determining the length dependence for the FR of MTs. In what follows, we shall quantify their influence individually, which then enables us to make the comparison between the TSE and IBE. In doing these, D/D_0 is plotted against the length L in Fig. 6 for fixed-free, fixed-fixed and free-free MTs, where TSE and IBE are considered, respectively. Here, to better demonstrate the correlation between the IBE and the FR, a method similar to the one used in Ref. [18] is employed to compute D/D_0 of MTs with the number of the blocked filaments ranging from 1 to 6. Fig. 6a shows that for the fixed-free MTs the IBE on the length dependence of the FR is much greater than TSE. For example, TSE raises D/D_0 from 0.75 to 1 (by 33.3 %) when L increases from 100 nm to 600 nm. After that, D/D_0 approaches 1 and remains unchanged when L further increases, i.e., TSE vanishes at $L > 600$ nm. However, when three filaments are blocked at the ends, IBE increases D/D_0 from 0.5 to 1 (by 100 %) in Fig. 6a. Significant length-dependence is achieved due to IBE for the FR until the MT length reaches 10 μm.

As for the fixed-fixed MTs, we find in Fig. 6b that TSE is predominant over IBE at $L <$ 300 nm. When the length falls in the range of $L > 300$ nm IBE surpasses TSE and plays a more important role in determining the length dependence of the FR. To give a specific example let us consider the fixed-fixed MT with three filaments blocked. We can see from Fig. 6b that, at $L <$ 300 nm TSE will decrease D/D_0 from 0.63 to 0.16 (by 74 %) as L declines from 300 nm to 100 nm. In the meantime, IBE will decrease D/D_0 from 0.63 to 0.41 (by 35 %). On the other hand,

when L > 300 nm is considered, the influence of TSE is small and disappears at L > 2 μm. However, IBE is still significant leading to D/D_0 = 0.9 when L increases up to 2 μm. The above analysis show that IBE is the major factor responsible for the length dependence of the FR of (fixed-free or fixed-fixed) MTs measured in experiments.

In Fig. 6c for the pinned-pinned MTs the length-dependence of D/D_0 due to TSE is calculated in comparison with the length dependence associated with IBE at $100\,\text{nm} \le L \le 10\,\mu\text{m}$. It is noted that although IBE is more significant than TSE, both of them disappear when L is around 1 μm or greater. This result is found to be in agreement with the experiments [10, 39], where the obtained FR is independent of MT length when the pinned-pinned boundary conditions are considered.

5. Conclusions

Based on MSM method and continuum mechanics model, we have studied the FR of MTs with different boundary conditions. Specifically, to accurately model the real boundary conditions imposed on MTs in experiments, in MSM simulations only a few filaments (instead of all filaments) are blocked at the ends and the kinesin is treated as an elastic body rather than a rigid body assumed in the previous study. Here, the elasticity of the kinesin is predicted based on the MM calculation. The simulations show that the length-dependence of the FR is significant for relatively short MTs, irrespective of their boundary conditions. However, for relatively long MTs usually measured in experiments the length dependence of the FR is found to dismiss in the free-free and pinned-pinned MTs but is detectable in the fixed-free and fixed-fixed MTs. This observation is consistent with the experimental observation. To capture the physics behind the boundary condition-selective length-dependent phenomenon of the FR, classic Timoshenko

beam model is modified by considering the general boundary conditions, where both TSE and IBE can be taken into account simultaneously. This modification enables one to compare TSE and IBE quantitatively. It is found that boundary condition-selective length-dependent phenomenon is primarily a result of IBE for MTs considered in experiments. In particular, the agreement between the experiments and the beam model shows that the newly developed beam model can be further employed to examine the influence of TSE and IBE on the mechanics of MTs.

Acknowledgements

This work was supported by the National Natural Science Foundation of China (No. 11602074). JZ also acknowledges the financial support from Harbin Institute of Technology (Shenzhen Graduate School) through the Scientific Research Starting Project for New Faculty.

Appendix

The dynamic equations for MTs modelled as the nonlocal Timoshenko beam can be expressed as [60]

$$K_s GA\left(\frac{\partial^2 w}{\partial x^2}+\frac{\partial \phi}{\partial x}\right)-\rho A\left(1-\left(e_0 a\right)^2\frac{\partial^2}{\partial x^2}\right)\frac{\partial^2 w}{\partial t^2}=0,$$

$$D\frac{\partial^2 \phi}{\partial x^2}-K_s GA\left(\frac{\partial w}{\partial x}+\phi\right)=0, \tag{6}$$

where $e_0 a$ is the scale coefficient that incorporates the small-scale effect.

The Timoshenko beam model for MTs developed based on the MCS theory can be written as [61]

$$K_s GA\left(\frac{\partial^2 w}{\partial x^2}+\frac{\partial \phi}{\partial x}\right)-\frac{1}{4}l^2 GA\left(\frac{\partial^4 w}{\partial x^4}-\frac{\partial^3 \phi}{\partial x^3}\right)-\rho A\frac{\partial^2 w}{\partial t^2}=0,$$

$$D\frac{\partial^2 \phi}{\partial x^2}-\frac{1}{4}l^2 GA\left(\frac{\partial^3 w}{\partial x^3}-\frac{\partial^2 \phi}{\partial x^2}\right)-K_s GA\left(\frac{\partial w}{\partial x}+\phi\right)=0, \quad (7)$$

where l is a material length scale parameter.

The frequency of MTs modelled by the above modified Timoshenko beam models can be solved numerically by the technique detailed in Sec. 3.

References

[1]. Hawkins, T., Mirigian, M., Yasar, M.S., Ross, J.L., J. Biomech. 43 (2010) 23.

[2]. Chretien, D., Fuller, S.D., J. Mol. Biol. 298 (2000) 663.

[3]. Alberts, B., Johnson, A., Lewis, J., Raff, M., Roberts, K., Walter, P., 2005. Molecular Biology of the Cell, 4th edition. Garland Science, New York.

[4]. Brangwynne, C.P., MacKintosh, F.C., Kumar, S., Giesse, N.A., Talbot, J., Mahadevan, L., Parker, K.P., Ingber, D.E., Weitz, D.A., J. Cell. Biol. 173 (2006) 733.

[5]. Howard, J., 2001. Mechanics of Motor Proteins and the Cytoskeleton, Sunderland, MA: Sinauer Associates.

[6]. Kis, A., Kasas, S., Babić, B., Kulik, A.J., Benoît, W., Briggs, G.A., Schönenberger, C., Catsicas, S., Forró, L., Phys. Rev. Lett. 89 (2002) 248101.

[7]. Felgner, H., Frank, R., Schliwa, M., J. Cell Sci. 109 (1996) 509.

[8]. Civalek, Ö., Demir, Ç., Appl. Math. Model. 35 (2011) 2053.

[9]. Kikumoto, M., Kurachi, M., Tosa, V., Tashiro, H., Biophys. J. 90 (2006) 1687.

[10]. Kawaguchi, K., Yamaguchi, A., Biochem. Biophys. Res. Commun. 402 (2010) 66.

[11]. Li, T., J. Biomech. 41 (2008) 1722.

[12]. Fu, Y.M., Zhang J., Physica E 42 (2010) 1741.

[13]. Gao, Y.W., Lei, F.M., Biochem. Biophys. Res. Commun. 387 (2009) 467.

[14]. Shen, H.S., Biomech. Model. Mechanobiol. 9 (2010) 345.

[15]. Shen, H.S., J. Theor. Biol. 264 (2010) 386.

[16]. Xiang, P., Liew, K.M., Int. J. Solids Struct. 48 (2011) 1730.

[17]. Akgöz, B., Civalek, Ö., Int. J. Mech. Sci. 81 (2014) 88.

[18]. Zhang, J., Wang, C.Y., Biomech. Model. Mechanobiol. 15 (2016) 1069.

[19]. Pokorný, J., Vedruccio, C., Cifra, M., Kučera, O., Eur. Biophys. J. 40 (2011) 747.

[20]. Gu, B., Mai, Y.W., Ru C.Q., Acta Mech. 207 (2009) 195.

[21]. Zeverdejani, M.K., Beni, Y.T., Curr. Appl. Phys. 13 (2013) 1566.

[22]. Beni, Y.T., Zeverdejani, M.K., J. Mech. Med. Biol. 15 (2015) 1550037.

[23]. Baninajjaryan, A., Beni, Y.T., J. Theor. Biol. 382 (2015) 111.

[24]. Xiang, P., Liew, K.M., Comput. Methods Appl. Mech. Eng. 223 (2012) 123.

[25]. Demir, Ç., Civalek, Ö., Appl. Math. Model. 37 (2013) 9355.

[26]. Qian, X.S., Zhang, J.Q., Ru, C.Q., J. Appl. Phys. 101 (2007) 84702.

[27]. Wang, J.B., Gao, Y.W., Appl. Math. Model. 40 (2016) 5731.

[28]. Daneshmand, F., Ghavanloo, E., Amabili, M., J. Biomech. 44 (2011) 1960.

[29]. Kurachi, M., Hoshi, M., Tashiro, H., Cell Motil. Cytoskeleton. 30 (1995) 221.

[30]. Felgner, H., Frank, R., Schliwa, M., J. Cell Sci. 109 (1996) 509.

[31]. Kis, A., Kasas, S., Kulik, A.J., Catsicas, S., Forró, L., Langmuir 24 (2008) 6176.

[32]. Venier, P., Maggs, A.C., Carlier, M.F., Pantaloni, D., J. Biol. Chem. 269 (1994) 13353.

[33]. Kurz, J. C., Williams Jr., R.C., Biochemistry 34 (1995) 13374.

[34]. Gittes, F., Mickey, B., Nettleton, J., Howard, J., J. Cell Biol. 120 (1993) 923.

[35]. Pampaloni, F., Lattanzi, G., Jonas, A., Surrey, T., Frey, E., Florin, E.L., Proc. Natl. Acad. Sci. USA 103 (2006) 10248.

[36]. Hawkins, T.L., Mirigian, M., Li, J., Yasar, M.S., Sackett, D.L., Sept, D., Ross, J.L., Cell Mol. Bioeng. 5 (2012) 227.

[37]. Hawkins, T.L., Sept, D., Mogessie, B., Straube, A., Ross, J.L., Biophys. J. 104 (2013) 1517.

[38]. Takasone, T., Juodkazis, S., Kawagishi, Y., Yamaguchi, A., Matsuo, S., Sakakibara, H., Nakayama, H., Misawa, H., Jpn. J. Appl. Phys. 41 (2002) 3015.

[39]. Gittes, F., Meyhofer, E., Baek, S., Howard, J., Biophys. J. 70 (1996) 418.

[40]. Kasas, S., Kis, A., Riederer, B.M., Forro, L., Dietler, G., Catsicas, S., Chem. Phys. Chem. 5 (2004) 252.

[41]. Zhang, J., Wang, C.Y., Biomech. Model. Mechanobiol. 13 (2014) 1175.

[42]. Zhang, J., Meguid, S.A., Appl. Phys. Lett. 105 (2014) 173704.

[43]. Ji, X.Y., Feng, X.Q., Phys. Rev. E 84 (2011) 031933.

[44]. Wade, R.H., Mol. Biotechnol. 43 (2009) 177.

[45]. Weaver Jr., W., Gere, J.M., 1990. Matrix Analysis of Framed Structures, 3rd edition. Van Nostrand Reinhold, New York.

[46]. Bornschlögl, T., Woehlke, G., Rief, M., Proc. Natl. Acad. Sci. USA 106 (2009) 6992.

[47]. Hariharan, V., Hancock, W.O., Cell Mol. Bioeng. 2 (2009) 177.

[48]. Kozielski, F., Sack, S., Marx, A., Thormahlen, M., Schonbrunn, E., Biou, V., Thompson, A., Mandelkow, E.M., Mandelkow, E., Cell 91 (1997) 985.

[49]. Rappe, A.K., Casewit, C.J., Colwell, K.S., Goddard, W.A., Skiff, W.M., J. Am. Chem. Soc. 114 (1992) 10024.

[50]. Rappe, A.K., Goddard, W.A., J. Phys. Chem. 95 (1991) 3358.

[51]. Adhikari, S., Flores, E.I.S., Scarpa, F., Chowdhury, R., Friswell, M.I., J. Nanotechnol. Eng. Med. 4 (2013) 041006.

[52]. Zeiger, A.S., Layton, B.E., Biophys. J. 95 (2008) 3606.

[53]. Chowdhury, R., Adhikari, S., Wang, C.Y., Scarpa, F., Comput. Mater. Sci. 48 (2010) 730.

[54]. Zhang, J., Wang, C.Y., Comput. Mater. Sci. 87 (2014) 26.

[55]. Deriu, M.A., Soncini, M., Orsi, M., Patel, M., Essex, J.W., Montevecchi, F.M., Redaelli, A., Biophys. J. 99 (2010) 2190.

[56]. Sept, D., MacKintosh, F.C., Phys. Rev. Lett. 104 (2010) 018101.

[57]. Wells, D.B., Aksimentiev, A., Biophys. J. 99 (2010) 629.

[58]. Weaver Jr., W., Timoshenko, S., Young, D.H., 1990. Vibration Problems in Engineering, 5th edition. Wiley, New York.

[59]. Bert, C.W., Malik, M., Appl. Mech. Rev. 49 (1996) 1.

[60]. Reddy, J., Pang, S., J. Appl. Phys. 103 (2008) 023511.

[61]. Ma, H.M., Gao, X.L., Reddy, J.N., J. Mech. Phys. Solids 56 (2008) 3379.

Tables

Table 1. The boundary condition-selective length dependence of the FR of MTs measured in different experiments.

Technique	Boundary conditions	Length dependence
Thermal fluctuation [35]; Laser trapping technique [38]	Fixed-free	Yes
Atomic force microscope [6, 31]	Fixed-fixed	Yes
Temperature pulse microscopy [10]	Pinned-pinned	No
Thermal fluctuation [36, 37]	Free-free	No

Table 2. Boundary conditions of the equivalent Timoshenko beam model for MTs with perfect or imperfect boundaries.

Boundary condition	Perfect	Imperfect
Free	$\frac{\partial \phi}{\partial x}=0;\ \frac{\partial w}{\partial x}+\phi=0$	-
Fixed	$\phi=0;\ w=0$	$-D\frac{\partial \phi}{\partial x}+k_{\theta}\phi=0;\ w=0$
Pinned	$\frac{\partial \phi}{\partial x}=0;\ w=0$	$\frac{\partial \phi}{\partial x}=0;\ K_{s}GA\left(\phi+\frac{\partial w}{\partial x}\right)+k_{x}w=0$

Figures

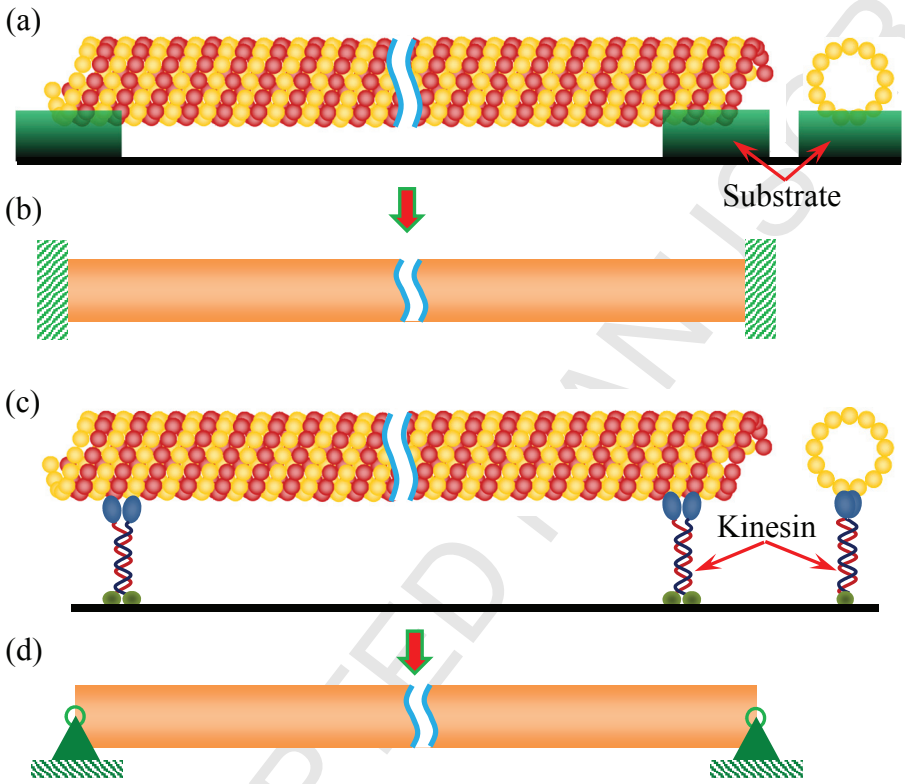

Fig. 1. (a) Atomic schematic and (b) equivalent continuum mechanics model of an MT deposited onto the surface of a substrate. (c) Atomic schematic and (d) equivalent continuum mechanics model of an MT linked to kinesin molecules.

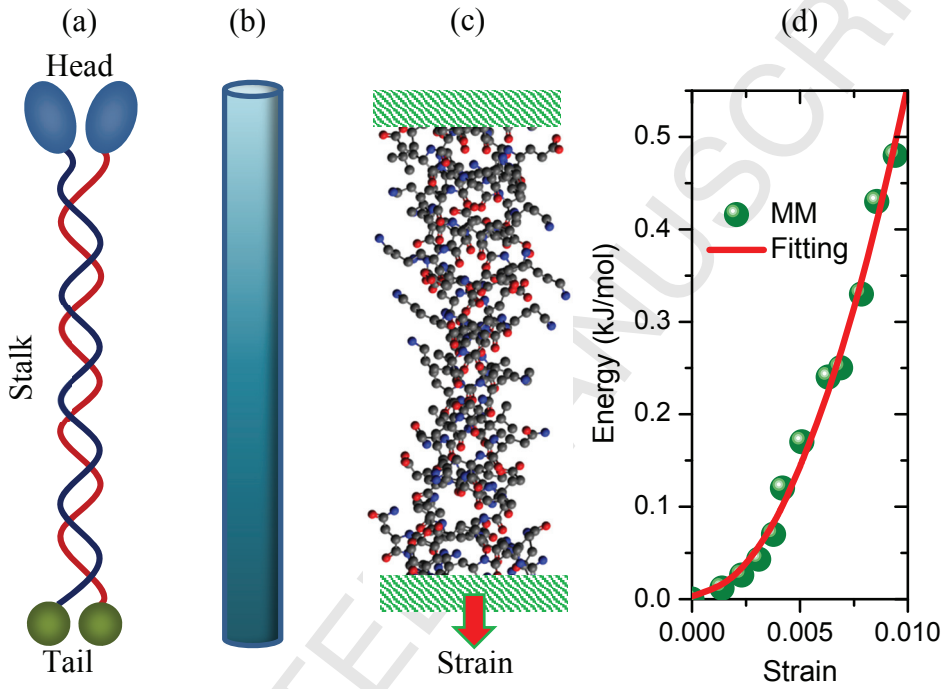

Fig. 2. (a) Structure schematic and (b) the equivalent bar model of the kinesin. (c) Simulation setup of the tensile test of the segment of the stalk. Here, the geometry of the segment of the stalk is taken from the standard protein data bank (PDB) file, 3KIN.pdb. (d) Variation of the total strain energies of the segment of the stalk with the axial strains.

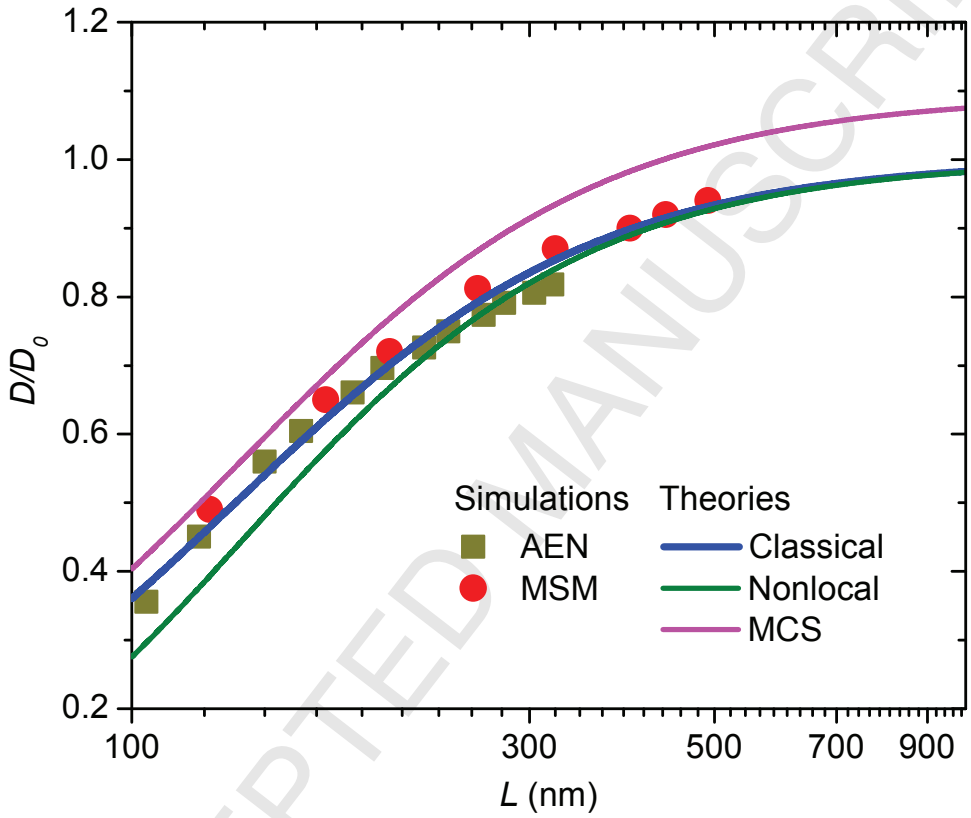

Fig. 3. Length (L)-dependent normalized FR (D/D_0) for free-free MTs calculated by various MM simulations (AEN and MSM methods) and various beam theories (classical beam models and beam models modified by nonlocal elasticity and MCS theories). Here, the AEN simulation results are adopted from Ref. [55].

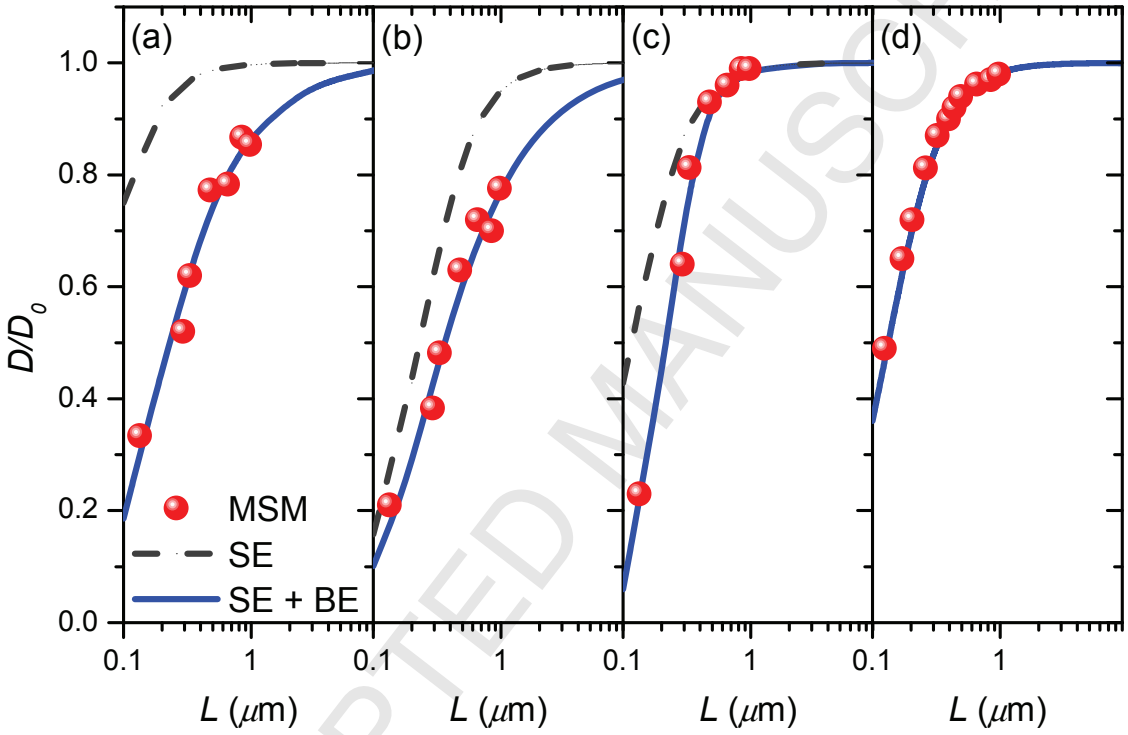

Fig. 4. Length-dependent normalized FR for (a) fixed-free, (b) fixed-fixed, (c) pinned-pinned and (d) free-free MTs calculated by MSM (symbols) and the continuum beam model only considering the influence of TSE (dashed lines) and considering the influence of both TSE and IBE (solid lines).

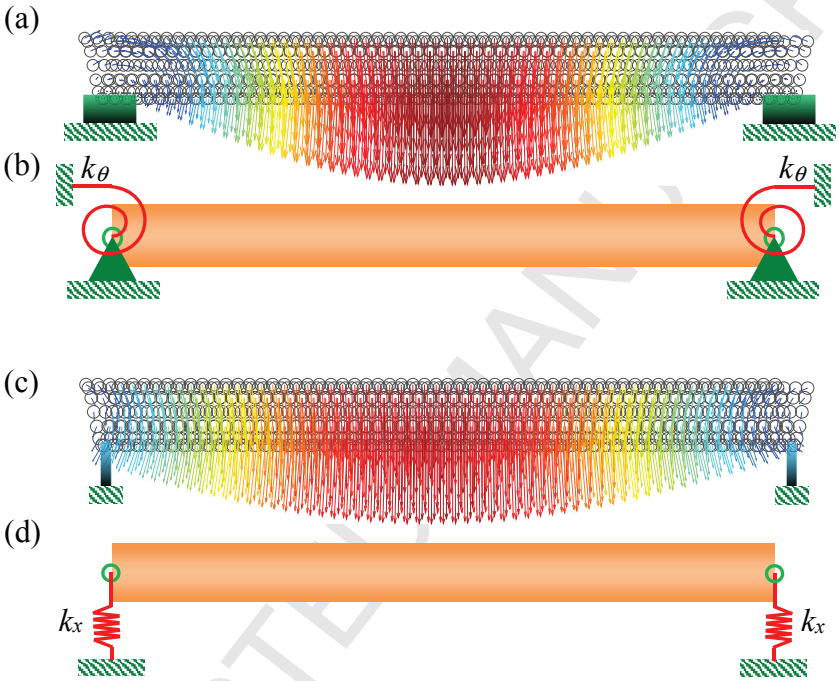

Fig. 5. (a) The displacement vector of the vibration mode of an MT, where a few filaments at the ends are blocked. (b) Continuum mechanics model of an MT supported by the torsional spring at the end. (c) The displacement vector of the vibration mode of an MT, whose ends are linked to the kinesin. (d) Continuum mechanics model of an MT supported by the linear spring at the end.

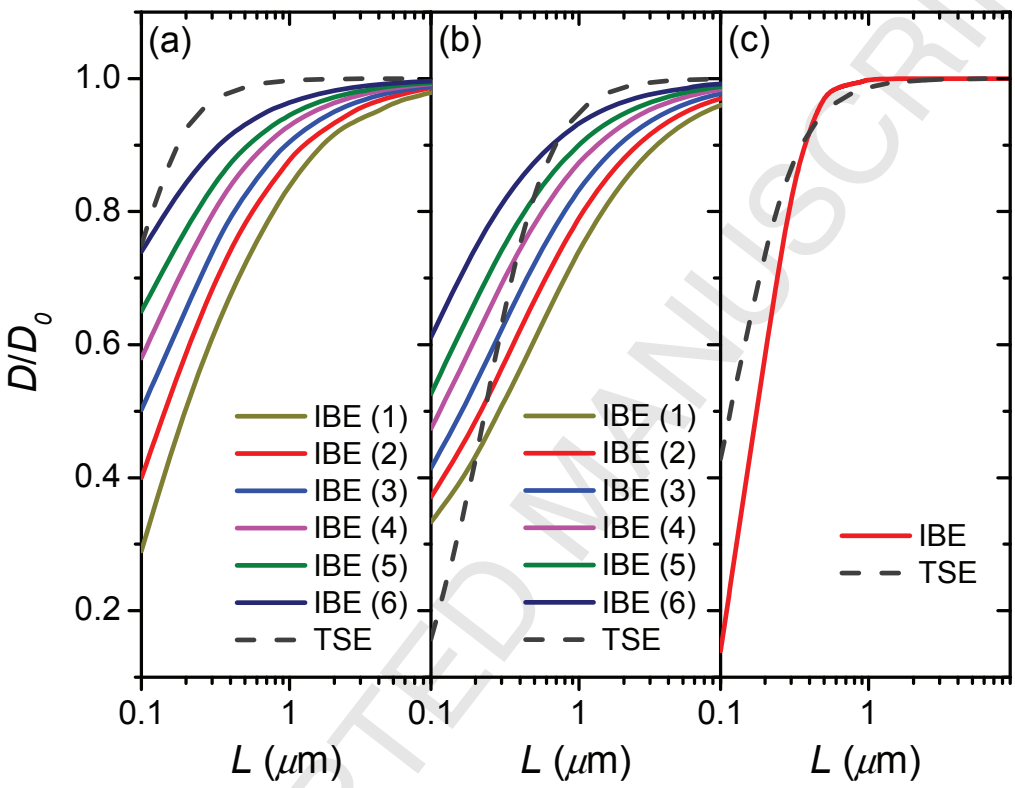

Fig. 6. Comparison between the contribution of TSE and IBE to the length-dependent normalized FR for (a) fixed-free, (b) fixed-fixed and (c) pinned-pinned MTs. The number in the blanket denotes the number of the blocked filaments at the ends of MTs.